Theor Ecol
DOI 10.1007/s12080-014-0225-9

ORIGINAL PAPER

Distinguishing intrinsic limit cycles from forced oscillations in ecological time series

Stilianos Louca · Michael Doebeli

Received: 21 January 2014 / Accepted: 3 April 2014

Abstract Ecological cycles are ubiquitous in nature and have triggered ecologists' interests for decades. Deciding whether a cyclic ecological variable, such as population density, is part of an intrinsically emerging limit cycle or simply driven by a varying environment is still an unresolved issue, particularly when the only available information is in the form of a recorded time series. We investigate the possibility of discerning intrinsic limit cycles from oscillations forced by a cyclic environment based on a single time series. We argue that such a distinction is possible because of the fundamentally different effects that perturbations have on the focal system in these two cases. Using a set of generic mathematical models, we show that random perturbations leave characteristic signatures on the power spectrum and autocovariance that differ between limit cycles and forced oscillations. We quantify these differences through two summary variables and demonstrate their predictive power using numerical simulations. Our work demonstrates that random perturbations of ecological cycles can give valuable insight into the underlying deterministic dynamics.

Keywords Ecological cycle · Environmental forcing · Noise · Autocovariance · Power spectrum · Decoherence

Electronic supplementary material The online version of this article (doi: 10.1007/s12080-014-0225-9) contains supplementary material, which is available to authorized users.

S. Louca (✉)
Institute of Applied Mathematics, University of British Columbia, 121-1984 Mathematics Road, Vancouver, BC, V6T 1Z2, Canada
e-mail: stilianos.louca@gmail.com

M. Doebeli
Department of Zoology, University of British Columbia, 6270 University Boulevard, Vancouver, BC, V6T 1Z4, Canada

Introduction

Ecological and epidemiological cycles have long been the subject of interest and controversy (Soper 1929; Elton and Nicholson 1942; Levy and Wood 1992; Ricker 1997; Trenberth 1997; Kendall et al. 1998; Grover et al. 2000; Krebs et al. 2001; Myers and Cory 2013). The underlying mechanisms causing such cycles are often hard to identify, in particular when the only available data is in form of a recorded time series. Commonly, suspected mechanisms are noise-sustained oscillations (Royama 1992; Kaitala et al. 1996; Nisbet and Gurney 2004), limit cycles arising from intrinsic ecological interactions (May 1972; Kendall et al. 1999; Gilg et al. 2003), and cyclic environmental forcing (Elton 1924; London and Yorke 1973; Sinclair et al. 1993; Hunter and Price 1998; García-Comas et al. 2011).

Noise-sustained oscillations can in principle be distinguished from intrinsic limit cycles and forced oscillations based on the system's probability distribution (Pineda-Krch et al. 2007), which describes how much time system trajectories spend in different areas of phase space. Discerning between limit cycles and forced oscillations is much harder, partly because the system's probability distribution is similar in both cases, namely concentrated along the cycle. Conventional approaches include autoregression analysis (Royama 1992), fitting generic, or system-specific mechanistic models to data (Turchin and Taylor 1992; Kendall et al. 1999), as well as cross-correlation and cross-spectral analysis of time series with hypothesized environmental driving forces (Sinclair et al. 1993; Stenseth et al. 2002). The first two methods implicitly assume an intrinsic mechanistic origin of the observed cycles, and it is not always clear at which point this assumption should be dropped in favor of an explanation involving periodic forcing. The third method

Published online: 10 May 2014

requires a concrete suspected driving force, to which the focal time series is to be compared.

Investigation of ecological cycles often involves their power spectrum (PS) or autocovariance (ACV), both standard concepts in time series analysis (Platt and Denman 1975; Royama 1992). The general perception is that forced cycles are characterized by a non-decaying autocovariance, i.e., a long-term temporal coherence, in contrast to intrinsic limit cycles (Berryman 2002; Nisbet and Gurney 2004). But this criterion implicitly assumes that any potential driving force would be temporally coherent or *phase-remembering* in Nisbet and Gurney's (2004) terminology. This is the case for the seasonal cycle, but is certainly not the general rule. For example, climatic cycles such as the El Niño-Southern Oscillation (Burgers 1999; Stenseth et al. 2002), the solar cycle (Sinclair et al. 1993; Klvana et al. 2004), and population cycles possibly causing fluctuations of coexisting focal species (Bulmer 1974) are typically phase forgetting, that is, exhibit low temporal coherence. Ecological variables driven by such cycles will clearly also be phase forgetting. Therefore, classifying ecological cycles as limit cycles solely based on a decaying autocovariance can lead to wrong conclusions.

In this article, we argue that a time series-based distinction between intrinsic limit cycles (LC) and forced oscillations (FO) is in principle possible when the focal variable is subject to random perturbations. The reason is that LCs and FOs respond qualitatively differently to noise, which shapes their power spectrum and autocovariance in characteristic ways. To the best of our knowledge, these qualitative but subtle differences have not been pointed out before in the context of distinguishing between LCs and FOs. Based on our observations, we propose a novel approach for classifying cyclic ecological variables as either part of a limit cycle or simply forced by one. We assume that other possibilities like noise-sustained oscillations and quasi-periodic chaos have been ruled out, and that the time series shows a single dominant spectral peak. We propose a set of unitless summary variables, V_{PS} and V_{ACV}, that are to be extracted from the estimated PS and ACV, and based on which a distinction between LC and FO becomes possible. We demonstrate their predictive power using numerical simulations of simple generic models for limit cycles and forced oscillations.

Theoretical background

Perturbations should reveal periodic forcing

In the following, we identify a periodic force or environmental parameter with the temporal variation it causes to the position of a stable node of the forced system. For example, the hypothetical effects of sockeye salmon population cycles (Ricker 1997) on zooplankton communities shall be seen as a periodic change in zooplankton equilibrium densities due to varying predation pressure.

The methods that we propose for classifying cyclic ecological variables as either part of intrinsic cycles or forced oscillations are based on the fundamentally different effects that random perturbations have on cycles in these two cases. Perturbations of forced oscillations are reversed by the forced system, which tends to stabilize on the equilibrium currently defined by the external driving force (Fig. 1a). Thus, perturbations of the focal ecological variable do not feed back into the driving force, and in particular do not influence the cycle's phase. In contrast, perturbations of limit cycles can cause random phase shifts along the cycle that are not reversed by the system's dynamics (Fig. 1b). The resulting stochastic phase drift leads to an increased spectral bandwidth and a decay of the system's autocovariance at larger time lags. These effects, known as jitter in electronic signal theory (Demir et al. 2000), result in the temporal decoherence of the cycle and a deviation from true periodicity. It is on these grounds that temporal decoherence has been perceived as a signature of limit cycles, as opposed to driven oscillations (Berryman 2002; Nisbet and Gurney 2004). However, as already pointed out, forced oscillations can also be decoherent when driven by decoherent cyclic forces. Hence, temporal decoherence by itself is generally not a sufficiently informative property.

Conceptually, deciding whether the focal ecological variable is part of a limit cycle or not translates to deciding whether the cycle's phase is causally affected by changes of the variable or not. Provided that the latter is subject to random perturbations, this question is equivalent to determining the extent to which these perturbations contribute to the cycle's decoherence. Stable systems driven by a cyclic

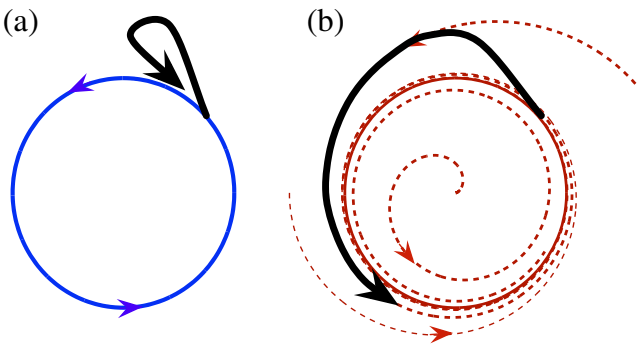

Fig. 1 On the fundamentally different effects of perturbations (first half of *thick arrow*) on forced oscillations (**a**) and intrinsic limit cycles (**b**). In the former case, perturbations tend to be reversed by the intrinsic dynamics of the forced system. In the latter case, perturbations have long-term effects on the cycle's phase

force will typically exhibit power spectra and autocovariances that relate to the ones of the driving force by means of their so called frequency transfer function and response function, respectively (Schetzen 2003; Nisbet and Gurney 2004). However, as discussed above, additional random perturbations are expected to modify their power spectra and autocovariances in characteristic ways that differ from perturbations that cause decoherence in the underlying cycle. It is these signatures that we attempt to quantify in the following section.

Considered models

As a limit cycle model, we consider the normal form of a supercritical Hopf bifurcation (Guckenheimer and Holmes 1985, Section 3.4), perturbed by additive Gaussian white noise. The Hopf bifurcation describes the emergence of a limit cycle around an unstable focus. It appears in a wide range of ecological and epidemiological models (Rosenzweig and MacArthur 1963; Greenhalgh 1997; Fussmann et al. 2000; Pujo-Menjouet and Mackey 2004), which is why we chose it as a generic model structure. We concentrate on a single model variable, denoted by L, because we wish to draw an analogy to ecological time series, which are often only available for a small subset of system variables, such as the population density of a single species. More precisely, we let

$$\begin{aligned}\frac{d}{dt}\begin{pmatrix} L \\ y \end{pmatrix} &= \begin{pmatrix} \lambda_1/2 & -\alpha_o \\ \alpha_o & \lambda_1/2 \end{pmatrix} \cdot \begin{pmatrix} L \\ y \end{pmatrix} \\ &+ \frac{(L^2+y^2)}{A^2}\begin{pmatrix} -\lambda_1 L/2 - (\alpha-\alpha_o)y \\ -\lambda_1 y/2 + (\alpha-\alpha_o)L \end{pmatrix} \\ &+ \sigma_1 \begin{pmatrix} \varepsilon_1 \\ \varepsilon_2 \end{pmatrix}, \end{aligned} \tag{1}$$

where y is a second variable coupled to L that is needed for the complete description of a limit cycle. The first row in Eq. 1 corresponds to the linear dynamics near the unstable focus, while the second row captures the nonlinearities giving rise to the limit cycle. Here, $\alpha > 0$, $A > 0$, and $\lambda_1 < 0$ are the limit cycle's angular frequency, amplitude, and negative Lyapunov exponent (or resilience), respectively, while $\alpha_o > 0$ is the system's angular frequency in the proximity of the focus. ε_1 and ε_2 are independent standard Gaussian white noise processes, and $\sigma_1 > 0$ is the noise amplitude. σ_1 quantifies the random perturbations of the cycle, such as weather events or demographic stochasticity in predator–prey cycles.

The power spectrum (PS) and autocovariance (ACV) of L can be approximated analytically when fluctuations around the limit cycle are weak ($\sigma_1^2 \ll A^2\lambda_1$) (Louca 2013, work in review). At any angular frequency ω, the PS is given by

$$\begin{aligned}\mathrm{PS}[L](\omega) \approx\ & A^2 F\left[\left(\frac{\sigma_1}{A}\right)^2, \alpha, \omega\right] \\ &+ \frac{\sigma_1^2}{2\lambda_1} F\left[\left(\frac{\sigma_1}{A}\right)^2 + 2\lambda_1, \alpha, \omega\right], \end{aligned} \tag{2}$$

where we defined

$$F[s,\alpha,\omega] := \frac{2s[4(\alpha^2+\omega^2)+s^2]}{[4(\alpha-\omega)^2+s^2][4(\alpha+\omega)^2+s^2]}.$$

The autocovariance of L at time lag τ is approximately

$$\begin{aligned}\mathrm{ACV}[L](\tau) \approx\ & \frac{1}{2}\left[A^2 + \frac{\sigma_1^2}{2\lambda_1} e^{-\lambda_1|\tau|}\right]\cos(\alpha\tau) \\ &\times \exp\left[-\frac{|\tau|\sigma_1^2}{2A^2}\right]. \end{aligned} \tag{3}$$

The exponential decay expressed in the second row of Eq. 3 quantifies the temporal decoherence of the cycle due to a Brownian motion-like phase drift along the deterministic trajectory. Figures 2a and b show the power spectrum and autocovariance estimated from a typical times series generated by such a noisy limit cycle, along with the expected values in Eqs. 2 and 3, respectively.

A forced ecological variable will respond approximately linearly to the variation of its equilibrium induced by the driving force, if this variation is sufficiently weak. We consider the simple case of a one dimensional linear system with resilience λ_s whose equilibrium is, after appropriate rescaling, identified with L:

$$\frac{dX}{dt} = -\lambda_s(X - L(t)) + \sigma_s\varepsilon. \tag{4}$$

Hence, X is driven by the cyclic variable $L(t)$, which is part of a perturbed limit cycle (Eq. 1) with variable perturbation strength. The amplitude σ_s of the additive Gaussian white noise in Eq. 4 quantifies the strength of non-decohering perturbations, such as the effects of short-term weather events on seasonally driven phytoplankton populations. In the deterministic limit ($\sigma_1 = \sigma_s = 0$), both the limit cycle in Eq. 1 and the driven system in Eq. 4 generate similar signals. In the stochastic case, it can be shown that the process given in Eq. 4 has the power spectrum

$$\mathrm{PS}[X](\omega) = \frac{\lambda_s^2}{\omega^2+\lambda_s^2}\cdot \mathrm{PS}[L](\omega) + \frac{\sigma_s^2}{\omega^2+\lambda_s^2} \tag{5}$$

and autocovariance

$$\begin{aligned}\mathrm{ACV}[X](\tau) =\ & \frac{\lambda_s}{2}\int_{\mathbb{R}} \mathrm{ACV}[L](u)\cdot e^{-\lambda_s|u-\tau|}\,du \\ &+ \frac{\sigma_s^2}{2\lambda_s} e^{-\lambda_s|\tau|} \end{aligned} \tag{6}$$

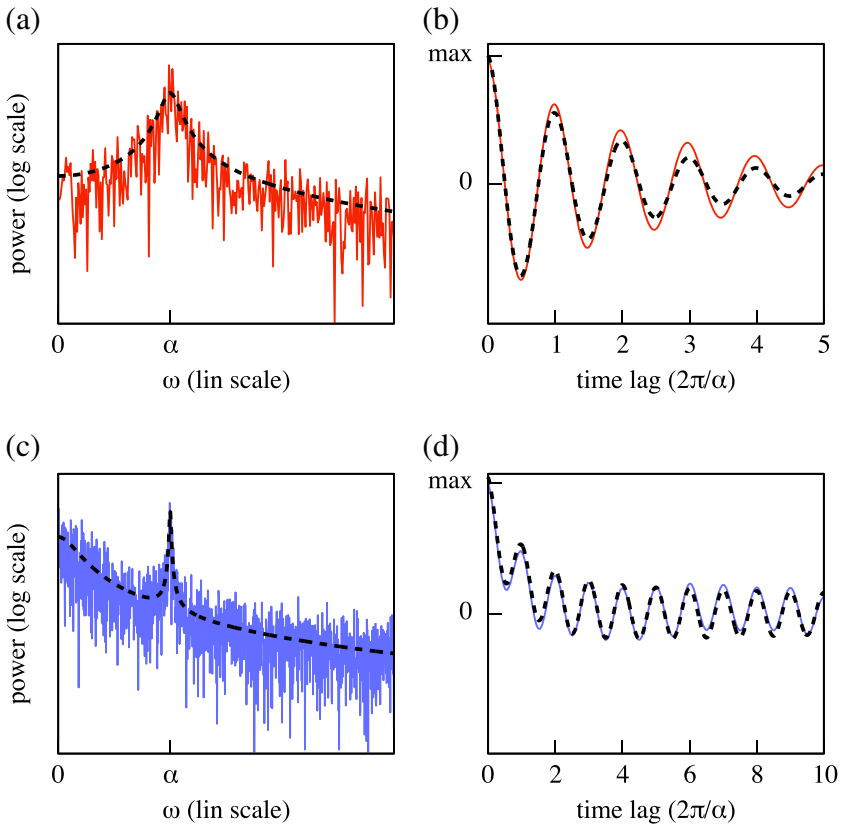

Fig. 2 **a** and **b** Power spectrum and autocovariance, respectively, estimated from time series generated using model (Eq. 1) for a noisy limit cycle of frequency α. **c** and **d** Power spectrum and autocovariance, respectively, estimated from time series using model (Eq. 4) for a stable linear system forced by a noisy limit cycle. *Black dashed curves* represent theoretical formulas (Eqs. 2 and 5) for the power spectra and the autocovariances, respectively. Parameter values given in Online Resource 1, Table 2

(Online Resource 1, Section 1). The modulation of the force's spectrum in Eq. 5 is due to the finite resilience λ_s of the forced system, which dampens high-frequency variations in L. Similarly, the convolution of ACV[L] in Eq. 6 expresses the memory of the forced system due to its finite resilience. For promptly responding systems ($\lambda_s \to \infty$), the first terms in Eqs. 5 and 6 become identical to PS[L] and ACV[L], respectively. In the general case, the integral in Eq. 6 becomes a complicated function of the model parameters (given in Online Resource 1, Section 1.3).

We are particularly interested in the right-most terms in Eqs. 5 and 6, originating in the non-decohering perturbations. These terms represent promising signatures of forced oscillations. Figures 2c and d show the power spectrum and autocovariance estimated from a typical time series generated by the model in Eq. 4, together with their theoretical values. The increased power at low frequencies seen in Fig. 2c, as well as the upward shift of the autocovariance at small time lags in Fig. 2d, are characteristic of forced oscillations, subject to non-decohering perturbations (Nisbet and Gurney 2004).

Classifier variables

The formulas for the expected power spectrum Eq. 5 and autocovariance Eq. 6 allow, at least in principle, an estimation of $A, \alpha, \sigma_l, \lambda_l, \sigma_s$, and λ_s from a cyclic time series, for example, through ordinary least squares fitting to the estimated power spectrum and autocovariance. Ideally, the right-most additive terms in Eqs. 5 and 6 should be estimated close to zero if the focal variable is part of an intrinsic limit cycle, and far from zero if the cyclic pattern results from cyclic forcing. In view of these expectations, we propose two summary variables of cyclic ecological time series:

$$V_{PS} = \frac{\sigma_s^2}{\lambda_s^2 PS(0)}, \quad V_{ACV} = \frac{\sigma_s^2}{2\lambda_s ACV(0)}.$$

V_{PS}, estimated for example by fitting Eq. 5, relates the power due to non-decohering perturbations to the total process power at zero frequency. V_{ACV}, estimated by fitting Eq. 6, relates the variance originating in non-decohering perturbations to the total variance. Both V_{PS} and V_{ACV} are expected to be distributed at higher values ($\lesssim 1$) in the case of forced oscillations (FO), and at lower values (≈ 0) for limit cycles (LC). Figure 3a, b show the estimated power spectrum and autocovariance of an El Niño-Southern Oscillation index (Trenberth 1997), along with fitted versions of Eqs. 5 and 6. The same is shown in Fig. 3 c, d for a summer temperature profile of Vancouver, clearly forced by the diurnal cycle. We chose these two textbook examples because their true nature is unambiguous. As seen in the figures, the two time series give values for V_{PS} and V_{ACV} compatible with our predictions.

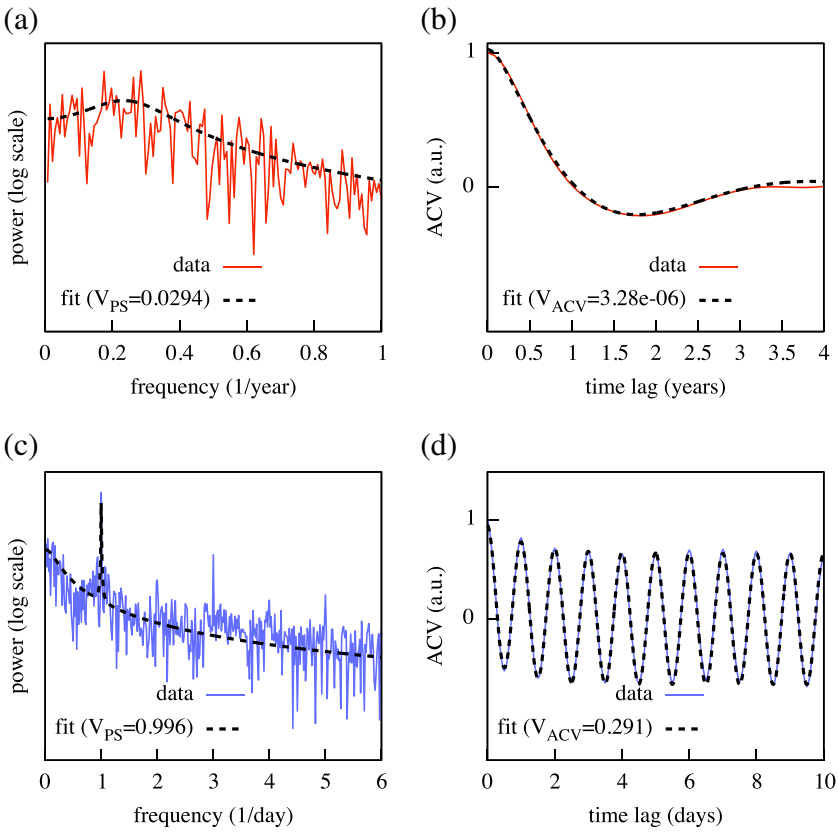

Fig. 3 **a** Power spectrum and **b** autocovariance of the El Niño N3.4 index between January 1871 and December 2007. The low values for V_{PS} and V_{ACV} (given in the figure legends) are in accordance with the oscillatory character of sea surface temperature, as part of the El Niño Southern Oscillation. **c** Power spectrum and **d** autocovariance of Vancouver temperature during July and August, 2013. The high values for V_{PS} and V_{ACV} reflect the forced character of the diurnal temperature oscillation. The *dashed curves* in all plots show the fitted formulas for the power spectrum in Eq. 5 and autocovariance in Eq. 6, from which V_{PS} and V_{ACV} were obtained. **a**, **b** were estimated from monthly data provided by NCAR CAS National Centre for Atmospheric Research (2007). **c**, **d** were estimated from hourly data provided by Environment Canada (2013)

We argue that V_{PS} and V_{ACV} are promising classifier variables that can be used in standard binary classification schemes for discerning limit cycles from forced oscillations (McLachlan 2004; Fradkin and Muchnik 2006). In practice, the distributions of V_{PS} and V_{ACV} for the two cases, LC and FO, are expected to overlap as a result of finite time series and estimation errors, therefore compromising the accuracy of any classifier based on them.

Numerical evaluation of V_{PS} and V_{ACV}

Methods

Using Monte Carlo simulations (Kroese et al. 2011), we evaluated the suitability of the summary variables V_{PS} and V_{ACV} for discerning between time series generated by the limit cycle model in Eq. 1 and the forced system in Eq. 4. Specifically, we examined the behavior of a simple threshold-based classification scheme based on any one of $V \in \{V_{PS}, V_{ACV}\}$, defined as follows: Depending on the value of V, estimated from some given time series, we

- classify the time series as a LC if $V \leq T_l$ (where T_l is some fixed threshold between 0 and 1),
- classify the time series as a FO if $V > T_u$ (where T_u is some fixed threshold between T_l and 1), and
- *reject* the case as *undetermined* if $T_l < V \leq T_u$.

Similar univariate classification schemes are widespread in diagnostic decision making (Dudoit et al. 2002; Pepe 2004).

The false FO detection rate (FDR) of such a classifier is defined as the fraction of LCs misclassified as FOs. Its true FO detection rate (TDR) is the fraction of FOs correctly classified as FOs. Its accuracy is the fraction of non-rejected cases that are correctly classified as either LC or FO. Varying the thresholds T_l and T_u changes the FDR, TDR, the rejection rate, and the classification accuracy. For example, a zero rejection rate is only achieved if $T_u = T_l$. In general, the FDR, TDR, rejection rate, and classification accuracy depend on the assumed probability of encountering a LC or FO. For our investigations, we took a non-biased approach and assumed both LC and FO to be equally likely. In principle, if the distributions of V_{PS} and V_{ACV} are known for LCs and FOs, the classification accuracy can be maximized by choice of T_l and T_u, whose difference should be sufficiently small for the rejection rate not to exceed a certain acceptable value.

Even if the rejection rate is zero ($T_l = T_u$), a tradeoff exists between reducing the FDR and increasing the TDR. The relationship between the FDR and TDR, as the classification threshold is varied, can be visualized using the

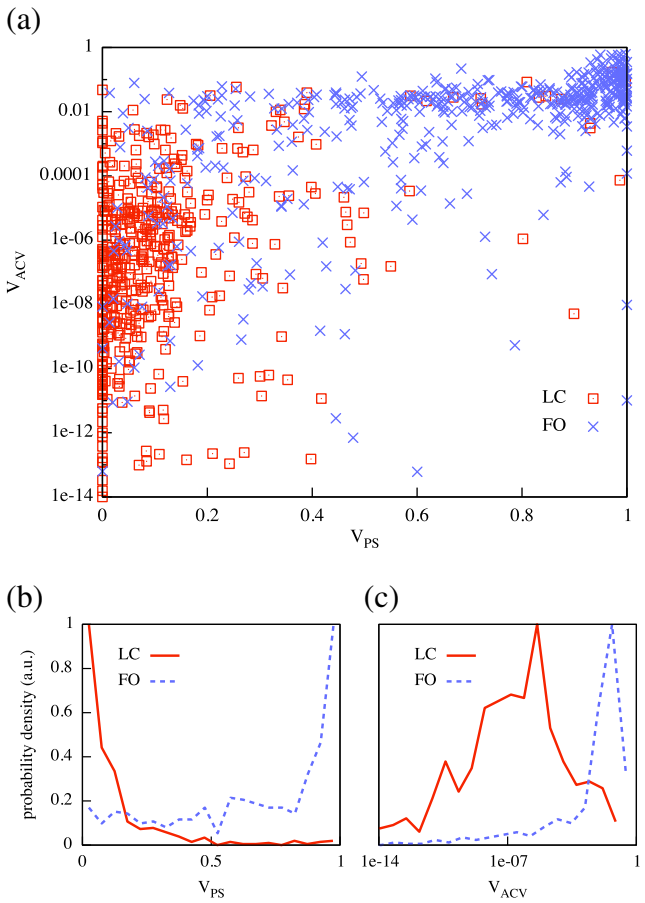

Fig. 4 **a** Scatterplot of the summary variables (V_{PS}, V_{ACV}) obtained from Monte Carlo simulations of the limit cycle model (Eq. 1) (*squares*) and the forced oscillation model (Eq. 4) (*crosses*) as described in the main text. **b** Corresponding estimated probability distributions of V_{PS} for limit cycles (*continuous line*) and forced oscillations (*dashed line*). **c** Corresponding estimated probability distributions of V_{ACV} for limit cycles (*continuous line*) and forced oscillations (*dashed line*). ROC curves calculated using the distributions shown in (**b**) and (**c**) are shown in Fig. 5a. Time series consisted of 200 points spanning across 20 cycle periods

so called receiver operating characteristic (ROC) (Brown and Davis 2006). The ROC curve is a widespread tool for the evaluation of threshold-based classifiers in signal detection theory and diagnostic decision making (Zweig and Campbell 1993). The area under the ROC curve (AUC), which ranges between 0.5 and 1.0, is often taken as a simple measure of the discriminative power of the classification variable, independently of any particular threshold. An AUC= 0.5 corresponds to no discriminative power at all and an AUC>0.8 is generally considered excellent (Hosmer 2013).

We sampled a large part of the entire 7-dimensional parameter space for the LC model and the FO model, generating an equal number of LC and FO time series of fixed size and duration. The considered parameter ranges are summarized in Online Resource 1, Table 1. We discarded cases that passed the D'Agostino-Pearson K^2 normality test (D'Agostino et al. 1990) with a significance above 0.05. This test evaluates the deviation of the phase-space distribution of trajectories from the normal distribution. A significant deviation from normality has been proposed as a criterion for ruling out noise-sustained oscillations as the cause of cycles (Pineda-Krch et al. 2007). We only considered cases whose estimated spectral peak had a statistical significance $P < 0.05$ (Scargle 1982; Horne and Baliunas 1986). For each run, we calculated V_{PS} and V_{ACV} by least squares fitting of Eqs. 5 and 6. We estimated the probability distributions of V_{PS} and V_{ACV} based on 1,000 runs. Using either V_{PS} or V_{ACV}, we calculated the maximum achievable accuracy of the classification scheme described above, by suitable choice of the thresholds T_l and T_u and for various rejection rates. We also constructed the ROC curves for the non-rejecting classifier ($T_l = T_u$) using either V_{PS} or V_{ACV}. Technical details are given in Online Resource 1, Section 2.

Results

Our simulations verified our predictions on the separate probability distributions of V_{PS} (or V_{ACV}) for LCs and FOs (Fig. 4a–c). The classification accuracy itself strongly depends on the quality (resolution and length) of the time series. For high-quality data (200 points across 20 cycle periods), the classification accuracy can reach almost 100 % for any of the two variables, given a sufficiently high rejection rate and an optimal choice of the classification thresholds T_l, T_u. For example, at a zero rejection rate, the maximum achievable accuracy exceeds 80 % for both V_{PS} and V_{ACV}. Accordingly, the ROC curves for the non-rejecting classifier exhibit a high AUC (>0.85 for both V_{PS} and V_{ACV}, Fig. 5a), underlining the strong discriminative power of V_{PS} and V_{ACV}. At a 30 % rejection rate, the maximum accuracy even exceeds 90 %.

For low-quality data (25 points across 5 cycle periods), the accuracy can drop by as much as 20 % and the AUC of the non-rejecting classifier can fall below 0.7 (Fig. 5b). The optimal classification thresholds were also found to slightly depend on the quality of the time series (Fig. 5), as well as on the considered range of model parameters. This is not surprising, since the probability distributions of V_{PS} and V_{ACV} depend not only on the distributions of model parameter values, but also on the accuracy of their estimation and therefore the quality of the time series.

It should be noted that power spectra estimated from time series are expected to show a flat background, should the sampling frequency be much lower than the system's resilience. This becomes clear in expression Eq. 5 for the power spectrum. In that case, fitted parameter values (in particular σ_l, σ_s) exhibit a high variance, thus compromising the

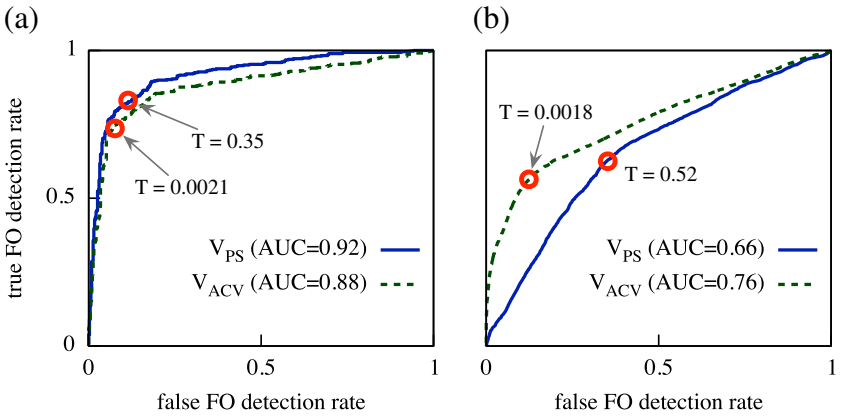

Fig. 5 Receiver operating characteristics for the non-rejecting (i.e., single-threshold) LC/FO classifiers using V_{PS} and V_{ACV}, for high-quality (**a**) and low-quality (**b**) time series. The area under the curve (AUC) is given in the figure legends and is a measure of the discriminative power of the considered variable. *Red circles* mark points of maximum classifier accuracy, with corresponding classification thresholds given adjacently. Time series consisted of 200 points and spanned 20 cycle periods in (**a**) and consisted of 25 points spanning 5 cycles in (**b**)

predictive power of V_{PS}. Similar issues arise for V_{ACV} when sampling durations are shorter than the typical correlation times of the limit cycle or of the forced system. Both of these effects have been observed in our Monte Carlo simulations.

Discussion

We have investigated the possibility of discerning intrinsic limit cycles from environmentally forced oscillations based on a single time series. Our proposed approach is superior to conventional procedures when neither an underlying limit cycle nor a periodic forcing can be excluded, and a concrete suspicion for a driving force as well as a mechanistic understanding of the studied system are both lacking. In our analysis, we did not require that cyclic environmental forces are temporally coherent, as is often (and often wrongfully) implicitly assumed. Hence, our reasoning also holds for cases where the periodic forcing itself results from a perturbed limit cycle exhibiting low temporal coherence.

We emphasize that care should be taken with the interpretation of signals classified as limit cycles. By construction, classifiers based on the summary variables V_{PS} and V_{ACV} can not differentiate between ecological variables undergoing forced oscillations but not subject to detectable perturbations, and dynamic variables bidirectionally coupled to a limit cycle. For example, the concentration of snowshoe hare droppings in northern Canada might be classified as part of a limit cycle, should a suitable time series be available (Krebs et al. 2001). However, this would be a result of the strong effects that hare populations have on dropping concentrations (i.e., droppings are a proxy for hares), and not because droppings themselves are part of a (putative) limit cycle.

In our models, we assumed that random perturbations are temporally uncorrelated. This assumption of white noise is only valid if environmental perturbations have short correlation times compared to the characteristic time scales of the studied ecosystem. It has been pointed out by several authors that environmental noise can show significant temporal correlations, particularly so in marine ecosystems (Steele 1985; Halley 1996; Halley and Inchausti 2004; Vasseur and Yodzis 2004). The differences in the power spectrum and autocovariance of limit cycles and forced oscillations, due to colored noise, remain to be investigated (see (Teramae et al. 2009) for some first results).

Our analysis is based on the assumption that quasi-periodic chaos has been ruled out as a possible cause of decoherent cyclicity. However, chaos is likely to occur in natural populations and has been proposed as an explanation for population-dynamical patterns like fluctuating vole populations (Turchin and Ellner 2000) and insect outbreaks (Dwyer et al. 2004). Identifying deterministic chaos in populations and distinguishing it from noise poses significant challenges and has long been subject to investigations (Hastings et al. 1993; Ellner and Turchin 1995; Cencini et al. 2000). Chaos is commonly detected in time series based on estimated Lyapunov exponents (Turchin and Ellner 2000; Kendall 2001; Becks et al. 2005; Beninca et al. 2008). Such non-parametric tests should precede the analysis proposed in this article when the system is suspected of being chaotic. Moreover, a poor fit of the theoretical power spectrum Eq. 5 and autocovariance Eq. 6 should always serve as an indicator of alternative mechanisms.

Complications are also expected for systems exhibiting multiple oscillatory mechanisms. For example, a combination of induced plant defenses and natural predation seems to explain forest insect outbreaks of alternating magnitude

(Elderd et al. 2013) and snowshoe hare cycles likely result from an interaction of predation and food supplies (Krebs et al. 2001). Furthermore, environmental seasonality can interact with nonlinear intrinsic processes and a complicated phase-space structure to produce irregular fluctuations, as demonstrated by models explaining seasonal measles outbreaks (Keeling et al. 2001) or the interannual variability of plankton community structure (Dakos et al. 2009). Prior estimation of the system's dimension (Abbott et al. 2009) can help avoid erroneous simplistic assumptions on the dynamics. Moreover, in many cases, different mechanisms leave characteristic signatures on the time series, such as separate peaks or higher harmonics in the power spectrum (Bjørnstad and Grenfell 2001; Hammer 2007; Elderd et al. 2013). Prior subtraction of secondary peaks, similar to the subtraction of long-term trends (Yamamura et al. 2006), might enable the analysis of isolated oscillatory mechanisms. However, we do not know how robust our analysis is against such data transformations. Ideally, the theory introduced here should be extended to these more complicated scenarios.

The anticipated practical value of V_{PS} and V_{ACV} in any classification scheme presumes a certain universality in their distribution for different systems, at least for systems whose limit cycles emerge through a supercritical Hopf bifurcation. In fact, the formulas (Eqs. 5 and 6) used to define V_{PS} and V_{ACV} are, strictly speaking, only meaningful for systems sharing a similar structure to Eqs. 1 and 4. We thus anticipate a low accuracy for cycles involving variables and perturbations at different scales of magnitude. More general versions of V_{PS} and V_{ACV} will be required to characterize such cases.

Regardless of the discriminative power of V_{PS} and V_{ACV}, choosing optimal classification thresholds is a non-trivial task that falls into the general category of classifier training (Alpaydin 2004). Thresholds determined from simulations of generic models, such as the ones presented here (Fig. 5), should serve as a starting point. Better results might be obtained through supervised learning using pre-classified time series from similar systems (e.g., using data from the Global Population Dynamics Database (NERC Centre for Population Biology 2010)), as is common in machine learning for medical diagnosis. For single-threshold classifiers, this translates to estimating the probability distributions of V_{PS} and V_{ACV} for typical ecological time series, based on which optimal thresholds can be determined.

Conclusions

Our exploratory work shows that the signatures of noise on ecological cycles can be used to distinguish variables contributing to the cyclic behavior from variables merely driven by it. The differences become particularly apparent in the summary variables V_{PS} and V_{ACV}, which quantify the stochasticity not directly affecting the cycle's phase. Moreover, the described approach has the potential to reveal the stability properties of the focal system as well as the amount of perturbations it is subject to. In the absence of experimental manipulations, naturally occurring perturbations and the transients they induce can therefore provide useful insights into a cycle's dynamics.

Acknowledgments This work was supported by the PIMS IGTC for Mathematical Biology and NSERC (Canada).

References

Abbott KC, Ripa J, Ives AR (2009) Environmental variation in ecological communities and inferences from single-species data. Ecology 90:1268–1278

Alpaydin E (2004) Introduction to machine learning. MIT Press

Becks L, Hilker FM, Malchow H, Jurgens K, Arndt H (2005) Experimental demonstration of chaos in a microbial food web. Nature 435:1226–1229

Beninca E, Huisman J, Heerkloss R, Johnk KD, Branco P, Van Nes EH, Scheffer M, Ellner SP (2008) Chaos in a long-term experiment with a plankton community. Nature 451:822–825

Berryman A (ed) (2002) Population cycles: the case for trophic interactions. Oxford University Press

Bjørnstad ON, Grenfell BT (2001) Noisy clockwork: time series analysis of population fluctuations in animals. Science 293:638–643

Brown CD, Davis HT (2006) Receiver operating characteristics curves and related decision measures: a tutorial. Chemometr Intell Lab Syst 80:24–38

Bulmer MG (1974) A statistical analysis of the 10-year cycle in canada. J Anim Ecol 43:701–718

Burgers G (1999) The El Niño stochastic oscillator. Clim Dyn 15:521–531

Cencini M, Falcioni M, Olbrich E, Kantz H, Vulpiani A (2000) Chaos or noise: Difficulties of a distinction. Phys Rev E 62:427–437

D'Agostino RB, Belanger A, D'Agostino RB (1990) A suggestion for using powerful and informative tests of normality. Am Stat 44:316–321

Dakos V, Benincà E, van Nes EH, Philippart CJM, Scheffer M, Huisman J (2009) Interannual variability in species composition explained as seasonally entrained chaos. Proc R Soc B: Biol Sci 276:2871–2880

Demir A, Mehrotra A, Roychowdhury J (2000) Phase noise in oscillators: a unifying theory and numerical methods for characterization. IEEE Trans Circ Syst I Fund Theor Appl 47:655–674

Dudoit S, Fridlyand J, Speed TP (2002) Comparison of discrimination methods for the classification of tumors using gene expression data. J Am Stat Assoc 97:77–87

Dwyer G, Dushoff J, Yee SH (2004) The combined effects of pathogens and predators on insect outbreaks. Nature 430:341–345

Elderd BD, Rehill BJ, Haynes KJ, Dwyer G (2013) Induced plant defenses, host–pathogen interactions, and forest insect outbreaks. Proc Natl Acad Sci USA 110:14,978–14,983

Ellner S, Turchin P (1995) Chaos in a noisy world: New methods and evidence from time-series analysis. Am Nat 145:343–375
Elton CS (1924) Periodic fluctuations in the numbers of animals: their causes and effects. J Exp Biol 2:119–163
Elton C, Nicholson M (1942) The ten-year cycle in numbers of the lynx in Canada. J Anim Ecol 11:215–244
Environment Canada (2013) Hourly temperature report, Station Vancouver Harbour CS. http://climate.weather.gc.ca, 17 January 2014
Fradkin D, Muchnik I (2006) Support vector machines for classification. DIMACS Ser Discret Math Theor Comput Sci 70:13–20. Citeseer
Fussmann GF, Ellner SP, Shertzer KW, Hairston NG (2000) Crossing the Hopf bifurcation in a live predator-prey system. Science 290:1358–1360
García-Comas C, Stemmann L, Ibanez F, Berline L, Mazzocchi MG, Gasparini S, Picheral M, Gorsky G (2011) Zooplankton long-term changes in the NW Mediterranean Sea: Decadal periodicity forced by winter hydrographic conditions related to large-scale atmospheric changes? J Mar Syst 87:216–226
Gilg O, Hanski I, Sittler B (2003) Cyclic dynamics in a simple vertebrate predator-prey community. Science 302: 866–868
Greenhalgh D (1997) Hopf bifurcation in epidemic models with a latent period and nonpermanent immunity. Math Comput Model 25:85–107
Grover J, McKee D, Young S, Godfray H, Turchin P (2000) Periodic dynamics in Daphnia populations: Biological interactions and external forcing. Ecology 81:2781–2798
Guckenheimer J, Holmes P (1985) Nonlinear oscillations, dynamical systems, and bifurcations of vector fields. Springer
Halley JM (1996) Ecology, evolution and 1/f-noise. Trends Ecol Evol 11:33–37
Halley JM, Inchausti P (2004) The increasing importance of 1/f-noises as models of ecological variability. Fluct Noise Lett 4:R1–R26
Hammer Ø (2007) Spectral analysis of a plio-pleistocene multispecies time series using the mantel periodogram. Palaeogeogr Palaeoclimatol Palaeoecol 243:373–377
Hastings A, Hom CL, Ellner S, Turchin P, Godfray HCJ (1993) Chaos in ecology: is mother nature a strange attractor? Annu Rev Ecol Syst 24:1–33
Horne JH, Baliunas SL (1986) A prescription for period analysis of unevenly sampled time series. Astrophys J 302:757–763
Hosmer D (2013) Applied logistic regression. Wiley, Sturdivant R
Hunter MD, Price PW (1998) Cycles in insect populations: Delayed density dependence or exogenous driving variables? Ecol Entomol 23:216–222
Kaitala V, Ranta E, Lindström J (1996) Cyclic population dynamics and random perturbations. J Anim Ecol 65:249–251
Keeling MJ, Rohani P, Grenfell BT (2001) Seasonally forced disease dynamics explored as switching between attractors. Phys D 148:317–335
Kendall BE (2001) Cycles, chaos, and noise in predator–prey dynamics. Chaos, Solitons Fractals 12:321–332
Kendall BE, Briggs CJ, Murdoch WW, Turchin P, Ellner SP, McCauley E, Nisbet RM, Wood SN (1999) Why do populations cycle? A synthesis of statistical and mechanistic modeling approaches. Ecology 80:1789–1805
Kendall BE, Prendergast J, Bjørnstad ON (1998) The macroecology of population dynamics: Taxonomic and biogeographic patterns in population cycles. Ecol Lett 1:160–164
Klvana I, Berteaux D, Cazelles B (2004) Porcupine feeding scars and climatic data show ecosystem effects of the solar cycle. Am Nat 164:283–297
Krebs CJ, Boonstra R, Boutin S, Sinclair AR (2001) What drives the 10-year cycle of snowshoe hares? Bioscience 51:25–35
Kroese D, Taimre T, Botev Z (2011) Handbook of Monte Carlo methods. Wiley Series in Probability and Statistics, Wiley
Levy D, Wood C (1992) Review of proposed mechanisms for sockeye salmon population cycles in the Fraser River. Bull Math Biol 54:241–261
London WP, Yorke JA (1973) Recurrent outbreaks of measles, chickenpox and mumps I. Seasonal variation in contact rates. Am J Epidemiol 98:453–468
May RM (1972) Limit cycles in predator-prey communities. Science 177:900–902
McLachlan GJ (2004) Discriminant analysis and statistical pattern recognition. Wiley Interscience
Myers JH, Cory JS (2013) Population cycles in forest lepidoptera revisited. Annu Rev Ecol Evol Syst 44:26.1–26.28
NCAR CAS National Centre for Atmospheric Research (2007) Niño 3.4 index. http://www.cgd.ucar.edu/cas/catalog/climind/TNI_N34/index.html, 15 January 2014
NERC Centre for Population Biology (2010) The global population dynamics database version 2. Online database available at: http://www3.imperial.ac.uk/cpb/databases/gpdd, 15 January 2014
Nisbet R, Gurney W (2004) Modelling fluctuating populations. Blackburn Press
Pepe M (2004) The statistical evaluation of medical tests for classification and prediction. Oxford statistical science series. Oxford University Press
Pineda-Krch M, J Blok H, Dieckmann U, Doebeli M (2007) A tale of two cycles–distinguishing quasi-cycles and limit cycles in finite predator–prey populations. Oikos 116:53–64
Platt T, Denman KL (1975) Spectral analysis in ecology. Annu Rev Ecol Syst 6:189–210
Pujo-Menjouet L, Mackey MC (2004) Contribution to the study of periodic chronic myelogenous leukemia. C R Biol 327:235–244
Ricker WE (1997) Cycles of abundance among Fraser River sockeye salmon (Oncorhynchus nerka). Can J Fish Aquat Sci 54:950–968
Rosenzweig ML, MacArthur RH (1963) Graphical representation and stability conditions of predator-prey interactions. Am Nat 97:209–223
Royama T (1992) Analytical population dynamics. Population and community biology series. Springer
Scargle JD (1982) Studies in astronomical time series analysis. II. Statistical aspects of spectral analysis of unevenly spaced data. Astrophys J 263:835–853
Schetzen M (2003) Linear time-invariant systems. Wiley
Sinclair AR, Gosline JM, Holdsworth G, Krebs CJ, Boutin S, Smith JN, Boonstra R, Dale M (1993) Can the solar cycle and climate synchronize the snowshoe hare cycle in Canada? Evidence from tree rings and ice cores. Am Nat:173–198
Soper H (1929) The interpretation of periodicity in disease prevalence. J R Stat Soc 92:34–73
Steele JH (1985) A comparison of terrestrial and marine ecological systems. Nature 313:355–358
Stenseth NC, Mysterud A, Ottersen G, Hurrell JW, Chan KS, Lima M (2002) Ecological effects of climate fluctuations. Science 297:1292–1296
Teramae Jn, Nakao H, Ermentrout GB (2009) Stochastic phase reduction for a general class of noisy limit cycle oscillators. Phys Rev Lett 102:194,102
Trenberth KE (1997) The definition of El Niño. Bull Am Meteorol Soc 78:2771–2777

Turchin P, Ellner SP (2000) Living on the edge of chaos: Population dynamics of fennoscandian voles. Ecology 81:3099–3116

Turchin P, Taylor AD (1992) Complex dynamics in ecological time series. Ecology 73:289–305

Vasseur DA, Yodzis P (2004) The color of environmental noise. Ecology 85:1146–1152

Yamamura K, Yokozawa M, Nishimori M, Ueda Y, Yokosuka T (2006) How to analyze long-term insect population dynamics under climate change: 50-year data of three insect pests in paddy fields. Popul Ecol 48:31–48

Zweig MH, Campbell G (1993) Receiver-operating characteristic (roc) plots: a fundamental evaluation tool in clinical medicine. Clin Chem 39:561–577

Distinguishing intrinsic limit cycles from forced oscillations in ecological time series

Supplementary material - Article submitted to Theoretical Ecology

Stilianos Louca[1] and Michael Doebeli[2]

[1] *Institute of Applied Mathematics, University of British Columbia, 121-1984 Mathematics Road, Vancouver, BC, V6T 1Z2, Canada, louca@math.ubc.ca*

[2] *Department of Zoology, University of British Columbia, 6270 University Boulevard, Vancouver, BC, V6T 1Z4 Canada,*

Abstract

This document is supplementary to the main article. We elaborate on our mathematical results and give details of numerical procedures.

1 Autocovariances and power spectra of forced linear systems

1.1 The n-dimensional case

In this section we derive formulas for the power spectrum and stationary autocovariance of stable linear systems with AGWN forced by some external signal. The effects of the forcing are identified with a temporal variability of the system's equilibrium $\mathbf{L}$. More precisely, we consider an n-dimensional system of the form

$$\frac{d\mathbf{X}}{dt} = \mathbb{A}(\mathbf{X} - \mathbf{L}(t)) + \mathbb{S}\mathbf{N}, \tag{1}$$

where $\mathbb{A} \in \mathbb{R}^{n\times n}$ is a stable matrix, $\mathbb{S} \in \mathbb{R}^{n\times n}$ is some matrix and $\mathbf{N}$ is an n-dimensional standard Gaussian white noise process. The sample paths of (1) are given by $\mathbf{X}(t) = \mathbf{X}_o(t) + \mathbf{Z}(t)$, where $\mathbf{Z}$ is an Ornstein-Uhlenbeck process

$$\frac{d\mathbf{Z}}{dt} = \mathbb{A}\mathbf{Z} + \mathbb{S}\mathbf{N}$$

and

$$\frac{d\mathbf{X}_o}{dt} = \mathbb{A}(\mathbf{X}_o - \mathbf{L}). \tag{2}$$

Hence, the power spectrum and autocovariance of the process $\mathbf{X}$ are given by

$$\mathrm{PS}[\mathbf{X}](\omega) = \mathrm{PS}[\mathbf{X}_o](\omega) + \mathrm{PS}[\mathbf{Z}](\omega)$$

and

$$\mathrm{ACV}[\mathbf{X}](\tau) = \mathrm{ACV}[\mathbf{X}_o](\tau) + \mathrm{ACV}[\mathbf{Z}](\tau),$$

respectively. The power spectrum and autocovariance of $\mathbf{Z}$ can be found in standard textbooks on the Ornstein-Uhlenbeck process (e.g. Gardiner 1985, Eq (4.4.58)).

Note that for the initial condition $\mathbf{X}_o|_{t=0} = 0$, (2) describes a time-invariant system with a linear response to the input $\mathbf{L}$, i.e. $\mathbf{X}_o = \mathbf{F}[\mathbf{L}]$ for some linear functional $\mathbf{F}$. As known from linear signal theory, its power spectrum and autocovariance can be related to that of $\mathbf{L}$ by means of its transfer function $\mathbb{T}(\omega) \in \mathbb{R}^{n\times n}$ and response function $\mathbb{H}(t) \in \mathbb{R}^{n\times n}$, respectively (Schetzen 2003). The latter is formally defined as $\mathbb{H}(t) = \mathbf{F}[\boldsymbol{\delta}](t)$, where $\boldsymbol{\delta}$ is the (vector valued) Dirac distribution at the origin. It satisfies $\mathbf{X}_o(t) = \int \mathbb{H}(t-s)\mathbf{L}(s)\, ds$. The transfer function is the Fourier transform of $\mathbb{H}$. One has

$$\mathrm{PS}[\mathbf{X}_o](\omega) = \mathbb{T}(\omega) \cdot \mathrm{PS}[\mathbf{L}](\omega) \cdot \mathbb{T}^\dagger(\omega) \tag{3}$$

where '$\dagger$' denotes the Hermitian conjugate, and

$$\mathrm{ACV}[\mathbf{X}_o](\tau) = \int_{\mathbb{R}}\int_{\mathbb{R}} \mathbb{H}(\mu) \cdot \mathrm{ACV}[\mathbf{L}](u) \cdot \mathbb{H}^\dagger(\mu + \tau - u)\, d\mu\, du. \tag{4}$$

In our case $\mathbb{H}(t) = -\Theta(t)e^{\mathbb{A}t}\mathbb{A}$, where $\Theta(t)$ is the Heaviside step function.

1.2 The one-dimensional case

We now turn to the one-dimensional case of (1), namely

$$\frac{dX}{dt} = -\lambda_\mathrm{s}(X - L(t)) + \sigma_\mathrm{s}N,$$

where $\lambda_\mathrm{s} > 0$ and $\sigma_\mathrm{s} \neq 0$. Then the response function and transfer function introduced in Section 1.1 take the form

$$H(t) = \Theta(t)\lambda_\mathrm{s}e^{-\lambda_\mathrm{s}t}, \quad T(\omega) = \frac{\lambda_\mathrm{s}}{\lambda_\mathrm{s} + i\omega}.$$

Hence, (3) and (4) take the forms

$$\mathrm{PS}[X_o](\omega) = \frac{\lambda_\mathrm{s}^2}{\omega^2+\lambda_\mathrm{s}^2}\cdot \mathrm{PS}[\mathbf{L}](\omega)$$

and

$$\mathrm{ACV}[X_o](\tau) = \frac{\lambda_\mathrm{s}}{2}\int_{\mathbb{R}} \mathrm{ACV}[L](u)\cdot e^{-\lambda_\mathrm{s}|u-\tau|}\,du, \quad (5)$$

respectively. Note that in the limit $\lambda_\mathrm{s}\to\infty$ (promptly reacting system), the power spectrum and autocovariance of X_o match the ones of the driving force L. The power spectrum and autocovariance of Z are given by

$$\mathrm{PS}[Z](\omega) = \frac{\sigma_\mathrm{s}^2}{\omega^2+\lambda_\mathrm{s}^2}, \quad \text{and} \quad \mathrm{ACV}[Z](\tau) = \frac{\sigma_\mathrm{s}^2}{2\lambda_\mathrm{s}} e^{-\lambda_\mathrm{s}|\tau|},$$

respectively (Xie 2006; Gillespie 1992). We can therefore summarize

$$\mathrm{PS}[X](\omega) = \frac{\lambda_\mathrm{s}^2}{\omega^2+\lambda_\mathrm{s}^2}\cdot \mathrm{PS}[\mathbf{L}](\omega) + \frac{\sigma_\mathrm{s}^2}{\omega^2+\lambda_\mathrm{s}^2},$$

and

$$\begin{aligned}\mathrm{ACV}[X](\tau) =& \frac{\lambda_\mathrm{s}}{2}\int_{\mathbb{R}} \mathrm{ACV}[L](u)\cdot e^{-\lambda_\mathrm{s}|u-\tau|}\,du \\ &+ \frac{\sigma_\mathrm{s}^2}{2\lambda_\mathrm{s}} e^{-\lambda_\mathrm{s}|\tau|}.\end{aligned}$$

1.3 Cyclic forcing

The autocovariance of a noisy limit cycle (see section of the main article) is given by

$$\begin{aligned}\mathrm{ACV}[L](\tau) \approx& \frac{1}{2}\Big[A^2 + \frac{\sigma_\mathrm{l}^2}{2\lambda_\mathrm{l}} e^{-\lambda_\mathrm{l}|\tau|}\Big]\cos(\alpha\tau) \\ &\times \exp\left[-\frac{|\tau|\,\sigma_\mathrm{l}^2}{2A^2}\right].\end{aligned}$$

In this case, the integral (5) can be evaluated explicitly using Mathematica (Wolfram Research 2010) and one obtains expression (6) shown below.

2 Numerical procedures

2.1 Monte Carlo simulations

We sampled the parameter ranges given in table 1 uniformly with 1000 independent runs. We used an explicit two-step Runge-Kutta scheme (Milstein 1995, §3.4, Theorem 3.3), implemented in C++. Time series were recorded at a constant time step δ. For each case, the variables V_PS and V_ACV, introduced in section of the main article, were calculated using the fitted parameters σ_s, λ_s and the fitted functions PS and ACV themselves (see Section 2.2). Given an acceptable rejection rate, the maximum achievable accuracy was estimated for the classifier proposed in section of the main article, using the empirical cumulative distribution functions for V_PS and V_ACV. We assumed an equal probability of limit cycles and forced oscillations.

Table 1: Parameter range used in the Monte Carlo simulations of the models (1) and (4) of the main article, as described in section of the main article. Without loss of generality we set $A = 1$ and $\alpha = 2\pi$. The limit cycle noise level was quantified by the standard deviation $\mathrm{SD_l} = \sqrt{\sigma_\mathrm{l}^2/(2\pi\alpha A^2)}$ in the probability distribution of the cycle phase within one cycle period (see Section 3 of this supplement). The noise of the forced system was quantified in a similar way.

Name	Symbol	Value range
Cycle amplitude	A	1
Cycle angular frequency	α	2π
Focal angular frequency	α_o	$\alpha/10$ – 10α
Limit cycle resilience	λ_l	$\alpha/(2\pi)$ – $10\alpha/(2\pi)$
Forced system resilience	λ_s	$\alpha/(2\pi)$ – $10\alpha/(2\pi)$
Limit cycle noise level	$\mathrm{SD_l}$	0.01 – 0.25
Forced system noise level	$\mathrm{SD_s}$	0.01 – 0.25

Table 2: Parameter ranges used in the simulations shown in figures 2(a–d) of the main article. Parameter descriptions are given in Table 1.

Symbol	fig. 2(a,b)	fig. 2(c,d)
A	1	1
α	1	1
α_o	1	1
λ_l	5	1
λ_s	–	1
$\sigma_\mathrm{l}^2/2$	0.5	0.2
$\sigma_\mathrm{s}^2/2$	–	0.04

2.2 Power spectra and autocovariances

Power spectra were estimated from time series using the Lomb-Scargle periodogram (Scargle 1982). We determined the significance of periodogram peaks against the null-hypothesis of white noise, as described by (Scargle 1982) and following the example of (Kendall et al 1998). Autocovariances were estimated by taking the inverse Fourier transform of the Lomb-Scargle periodogram, similar to the method described by Rehfeld et al (2011). All fitting was done using ordinary least-squares with ALGLIB (Bochkanov 2013) (on a logarithmic scale for the PS). We dismissed cases where the periodogram peak was more than 50% away from the anticipated frequency

$$
\begin{aligned}
\mathrm{ACV}[X](\tau) = {} & \frac{A^2}{2\lambda_\mathrm{l}} e^{-\lambda_\mathrm{s}|\tau|} \lambda_\mathrm{s} \Bigg\{ 1 + \frac{A^2\lambda_\mathrm{l}\left(-2A^2\lambda_\mathrm{s} + \sigma_\mathrm{l}^2\right)}{4A^4\left(\alpha^2 + \lambda_\mathrm{s}^2\right) - 4A^2\lambda_\mathrm{s}\sigma_\mathrm{l}^2 + \sigma_\mathrm{l}^4} + \frac{A^2\lambda_\mathrm{l}\left(2A^2\lambda_\mathrm{s} + \sigma_\mathrm{l}^2\right)}{4A^4\left(\alpha^2 + \lambda_\mathrm{s}^2\right) + 4A^2\lambda_\mathrm{s}\sigma_\mathrm{l}^2 + \sigma_\mathrm{l}^4} \\
& + \frac{-2A^4\left(\alpha^2 + (\lambda_\mathrm{s} - \lambda_\mathrm{l})^2\right) + A^2(\lambda_\mathrm{s} - \lambda_\mathrm{l})\sigma_\mathrm{l}^2}{4A^4\left(\alpha^2 + (\lambda_\mathrm{s} - \lambda_\mathrm{l})^2\right) + 4A^2(-\lambda_\mathrm{s} + \lambda_\mathrm{l})\sigma_\mathrm{l}^2 + \sigma_\mathrm{l}^4} - \frac{2A^4\left(\alpha^2 + (\lambda_\mathrm{s} + \lambda_\mathrm{l})^2\right) + A^2(\lambda_\mathrm{s} + \lambda_\mathrm{l})\sigma_\mathrm{l}^2}{4A^4\left(\alpha^2 + (\lambda_\mathrm{s} + \lambda_\mathrm{l})^2\right) + 4A^2(\lambda_\mathrm{s} + \lambda_\mathrm{l})\sigma_\mathrm{l}^2 + \sigma_\mathrm{l}^4} \\
& + 2A^2 e^{-\lambda_\mathrm{l}|\tau| - \frac{\sigma_\mathrm{l}^2|\tau|}{2A^2}} \lambda_\mathrm{s} \Bigg[\\
& - \frac{e^{\lambda_\mathrm{s}|\tau|}\sigma_\mathrm{l}^2\left(-4A^4\left(\alpha^2 + \lambda_\mathrm{s}^2 - \lambda_\mathrm{l}^2\right) + 4A^2\lambda_\mathrm{l}\sigma_\mathrm{l}^2 + \sigma_\mathrm{l}^4\right)\cos(\alpha\tau)}{16A^8\left(\left(\alpha^2 + \lambda_\mathrm{s}^2\right)^2 + 2(\alpha^2 - \lambda_\mathrm{s}^2)\lambda_\mathrm{l}^2 + \lambda_\mathrm{l}^4\right) + 32A^6\lambda_\mathrm{l}\left(\alpha^2 - \lambda_\mathrm{s}^2 + \lambda_\mathrm{l}^2\right)\sigma_\mathrm{l}^2 + 8A^4\left(\alpha^2 - \lambda_\mathrm{s}^2 + 3\lambda_\mathrm{l}^2\right)\sigma_\mathrm{l}^4 + 8A^2\lambda_\mathrm{l}\sigma_\mathrm{l}^6 + \sigma_\mathrm{l}^8} \\
& + \frac{4A^2 e^{\lambda_\mathrm{s}|\tau|}\alpha\sigma_\mathrm{l}^2\left(2A^2\lambda_\mathrm{l} + \sigma_\mathrm{l}^2\right)\sin(\alpha\tau)}{16A^8\left(\left(\alpha^2 + \lambda_\mathrm{s}^2\right)^2 + 2(\alpha^2 - \lambda_\mathrm{s}^2)\lambda_\mathrm{l}^2 + \lambda_\mathrm{l}^4\right) + 32A^6\lambda_\mathrm{l}\left(\alpha^2 - \lambda_\mathrm{s}^2 + \lambda_\mathrm{l}^2\right)\sigma_\mathrm{l}^2 + 8A^4\left(\alpha^2 - \lambda_\mathrm{s}^2 + 3\lambda_\mathrm{l}^2\right)\sigma_\mathrm{l}^4 + 8A^2\lambda_\mathrm{l}\sigma_\mathrm{l}^6 + \sigma_\mathrm{l}^8} \\
& + \frac{2A^2 e^{(\lambda_\mathrm{s}+\lambda_\mathrm{l})|\tau|}\lambda_\mathrm{l}\left(\left(4A^4\left(\alpha^2 + \lambda_\mathrm{s}^2\right) - \sigma_\mathrm{l}^4\right)\cos(\alpha\tau) + 4A^2\alpha\sigma_\mathrm{l}^2\sin(\alpha\tau)\right)}{16A^8\left(\alpha^2 + \lambda_\mathrm{s}^2\right)^2 + 8A^4(\alpha^2 - \lambda_\mathrm{s}^2)\sigma_\mathrm{l}^4 + \sigma_\mathrm{l}^8} \Bigg] \Bigg\} \\
& + \frac{\sigma_\mathrm{s}^2}{2\lambda_\mathrm{s}} e^{-\lambda_\mathrm{s}|\tau|}.
\end{aligned}
\tag{6}
$$

α, because of technical issues in the peak detection algorithm.

3 Phase effects of noise

In this section we elaborate on the effects that noise is expected to have on the coherence of limit cycles. The phase of a limit cycle perturbed by weak AGWN drifts away from its deterministic value approximately in a Brownian-motion-like manner (Louca 2013, work in review). As a result, the phase probability distribution is approximately a Gaussian with a variance $\nu^2(t)$ that increases with time. For a limit cycle of length C and period T, advancing at uniform speed in phase space and subject to isotropic AGWN of variance σ^2, one has

$$\nu^2(T) = T\frac{\sigma^2}{C^2}$$

(assuming a fixed phase at time $t = 0$ and a 1-periodic phase coordinate). For our Monte Carlo simulations, we quantified the noise level by the resulting variance, $\mathrm{SD}^2 = \sigma/(2\pi\alpha A^2)$, of the phase of a limit cycle of radius A and angular frequency α, after one cycle period.

References

Bochkanov S (2013) Alglib 3.8.0. Available at: http://www.alglib.net (Jan 15, 2014)

Gardiner CW (1985) Handbook of stochastic methods for physics, chemistry and the natural sciences. Springer

Gillespie D (1992) Markov Processes: An Introduction for Physical Scientist. Academic Press

Kendall BE, Prendergast J, Bjørnstad ON (1998) The macroecology of population dynamics: taxonomic and biogeographic patterns in population cycles. Ecol Lett 1:160–164

Milstein G (1995) Numerical Integration of Stochastic Differential Equations. Mathematics and its Applications, Kluwer, Dordrecht, The Netherlands

Rehfeld K, Marwan N, Heitzig J, Kurths J (2011) Comparison of correlation analysis techniques for irregularly sampled time series. Nonlinear Processes Geophys 18:389–404

Scargle JD (1982) Studies in astronomical time series analysis. II. Statistical aspects of spectral analysis of unevenly spaced data. Astrophys J 263:835–853

Schetzen M (2003) Linear Time-Invariant Systems. Wiley

Wolfram Research I (2010) Mathematica, version 8.0 edn. Wolfram Research, Inc., Champaign, Illinois

Xie WC (2006) Dynamic Stability of Structures. Cambridge University Press